ChemComm

Accepted Manuscript

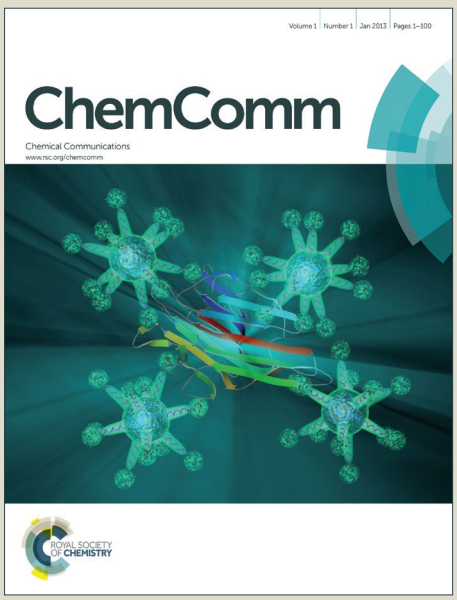

ROYAL SOCIETY OF CHEMISTRY

www.rsc.org/chemcomm

Journal Name

COMMUNICATION

Boronate Affinity Molecularly Imprinted Inverse Opal Particles for Multiple Label-Free Bioassays

Received 00th January 20xx,
Accepted 00th January 20xx

DOI: 10.1039/x0xx00000x

www.rsc.org/

Huan Wang,[a] Qionghua Xu,[a] Luoran Shang,[a] Jie Wang,[a] Fei Rong,*[ab] Zhongze Gu*[ab] and Yuanjin Zhao*[ab]

Boronate affinity molecularly imprinted polymer inverse opal particles were developed for the multiplex label-free detection of glycoproteins with a high sensitivity and specificity.

Multiplex bioassays, biotechnologies with the ability to detect multiple biomolecular targets in a single sample simultaneously, are very important for clinical diagnosis, gene expression, drug discovery and so on[1]. One successful technology developed in this field is suspension arrays[2], which use barcode particles as elements for multiplexing. Compared with conventional planar arrays[3], these barcode particle-based suspension arrays show high flexibility, fast reaction, good reproducibility and high sensitivity for detecting[4]. Many encoding strategies have been proposed for the suspension barcode particles, including incorporation of segmented nanorods, photopatterning, fluorescent colloids, photonic crystals (PhCs) and so on[5]. Among them, PhC barcode particles hold immense promise for suspension arrays because of their excellent optical properties, such as minimal spectral width, remarkable stability, and freedom from fluorescent background. However, during the immunoassay applications of the suspension arrays, including the PhC barcode particle arrays, attaching to the target molecules are usually unavoidable in target analysis by detecting fluorescence or absorbance labels[6]. In addition to the high cost imposed by reagents and instruments, the labels or labeling itself will hinder the interactions and the activity of biomolecules, which could lead to false negative detection results. Moreover, the immune-antibody storage stability, high cost, and difficulties associated with their production, together with the loss of biological activity upon external treatment, are often cited as problems. Therefore, it is highly desirable to develop antibody- and label-free detection in the barcode suspension assay.

In this paper, we present a novel strategy for the desired detection by boronate affinity molecularly imprinted polymer (MIP) PhC barcode particles. MIPs are economical and stable synthetic receptors with antibody-like binding properties. They were employed as artificial antibodies and have found important applications in the detection of biomolecules based on their physicochemical responses, such as changes in refractive index and volume[7]. In particular, with the boronate affinity as the functional elements, the MIPs exhibit many attractive characteristics, such as reversible binding, high affinity, high specificity, and superb tolerance to interference[8]. These features make them appealing alternatives to antibodies for immunoassays[9] and glycoproteomics[10]. However, the potential value of the boronate affinity MIPs for the construction of the barcode suspension assay is still unexplored. Thus, we herein employed them as the elements of the PhC barcode particles and investigated the responsive of these particles to different glycoproteins. The specific binding of the glycoproteins in the imprinted boronate affinity nanocavities of the PhC barcode particles cause the MIPs swelling and this is detected as a corresponding shift in the Bragg diffraction peak position, which could be used for quantitatively estimating the amount of bound biomolecules[11]. Based on this principle, the feasibility of antibody- and label-free multiplex detection of glycoproteins could be realized in the barcode suspension assay.

In a typical experiment, silica colloidal crystal beads (SCCBs) were employed as templates for the fabrication of the MIP PhC barcode particles. The principle and procedure of this fabrication process is outlined in Scheme 1. Briefly, the hydrophilically modified SCCBs (Scheme 1a) were immersed in the MIP pregel solution at first. The mixture was then polymerized under ultra violet (UV) light after the void spaces between the silica nanoparticles of the SCCBs were fully SCCBs (Scheme 1b) were collected from the polymerized hydrogel by swelling and tearing the bulk hydrogel. Finally, the inverse opal structured MIP particles were obtained after removal of the template SCCBs and imprinted molecules.

[a] State Key Laboratory of Bioelectronics, School of Biological Science and Medical Engineering, Southeast University, Nanjing 210096, China. E-mail: yjzhao@seu.edu.cn; gu@seu.edu.cn
[b] Laboratory of Environment and Biosafety, Research Institute of Southeast University in Suzhou, Suzhou 215123, China E-mail: rong@seu.edu.cn;
Electronic Supplementary Information (ESI) available: Experimental details, the metalloscope images of blue and red particles, the results of RNase B and TRF detection. See DOI: 10.1039/x0xx00000x

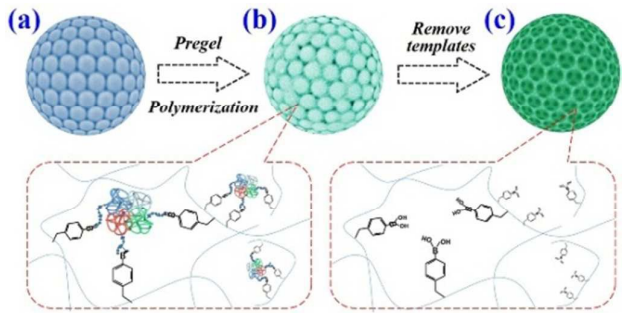

Scheme 1 Schematic diagram of the preparation process of the molecular imprinted polymer (MIP) PhC barcode particles.

In this research, the MIP pregel solution was mainly composed of polyethylene glycol diacrylate (PEGDA), 4-vinylphenylboronic acid (VPBA), and imprinted target molecules. The VPBA is a kind of functional monomer, which can covalently bind cis-diol-containing molecules such as sugars and glycoproteins to form stable cyclic esters in alkaline aqueous solution, while the boronate esters dissociate and the cis-diol-containing molecules are released when the surrounding pH is switched to acidic. Both the PEGDA and VPBA are photocurable and can form stable hydrogel gridding to immobilize the complex of the functional VPBA and the imprinted targets. Thus, the inverse opal structured MIP particles were imparted with precisely positioned boronic groups and "footprints" of the imprinted target molecules in their macroporous hydrogel scaffolds (Scheme 1c) when the template silica nanoparticles and the imprinted molecules were removed.

The microstructure of the template SCCBs and the replicated MIP inverse opal particles was observed by scanning electron microscopy, as shown in Fig. 1. It was observed that the silica nanoparticles on the surface of the template SCCBs formed a hexagonal alignment (Fig. 1a) and this ordered array structure also extended to the inside of the SCCBs (Fig. 1b). Thus, the MIP hydrogel particles replicated from the SCCBs should have a similar highly three-dimensional (3D) ordered inverse opal structure. This was primarily confirmed by images of the MIP hydrogel hybrid SCCBs, which indicated that the MIP hydrogel had efficiently filled the voids in the SCCB templates (Fig. 1c). However, the desired inverse opal nanostructure was difficult to be observed due to the shrinking and collapsing during the drying process of the soft MIP scaffolds (Fig. 1d). Thus, to further investigate the actual nanostructure of the replaced MIPs, a high concentration of the PEGDA was employed to maintain the MIP hydrogel scaffolds during their drying. As expected, a porous surface of the improved hydrogel inverse opal particles was observed. The pores formed a mainly hexagonal symmetrical pattern, and were also interconnected and extended inside the inverse opal hydrogel particles (Fig. 1e and 1f). This structure can offer easier access for the target molecules to the boronic groups imprinted "footprints".

Because of the ordered nanostructure, the template SCCBs and the replicated MIP inverse opal particles were imparted with a photonic band gap (PBG) property and show the corresponding structural color or characteristic reflection peak (Fig. 2 and Fig. S1). Under normal incidence, the peak positions λ of the MIP inverse opal particles can be estimated by Bragg's equation:

$$\lambda = 1.633 d n_{average} \quad (1)$$

where d is the center-to-center distance between two neighboring nanopores, and $n_{average}$ is the average refractive index of the particles. Therefore, by changing the diameters of the silica nanoparticles and their derived pores, a series of MIP inverse opal particles with different diffraction-peak positions and colors could be obtained (Fig. 2d), which can be derived for encoding. It was worth mentioning that the reflection peaks of the MIP inverse opal particles were flexible and changeable when their MIP hydrogels were integrated with stimulus-responsive elements, such as their imprinted target molecules. Although the target molecules could cause a slight

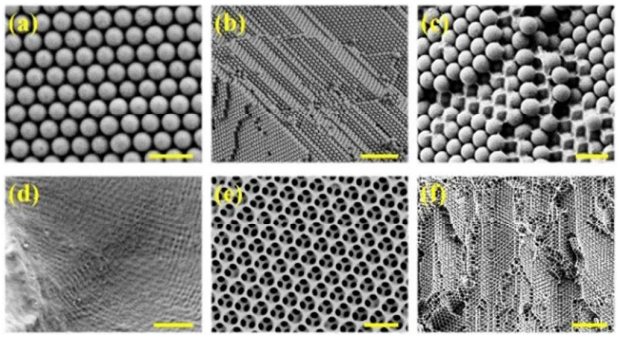

Fig. 1 SEM images of the SCCBs and the MIP inverse opal particles: (a, b) surface and inner microstructures of a template SCCB; (c) microstructure of a hydrogel hybrid SCCB; (d) surface image of a collapsing MIP particle; (e, f) surface and inner microstructures of an inverse opal hydrogel particles. Scale bars are 500 nm in (a, c, e), 1 μm in (d), and 2 μm in (b, f).

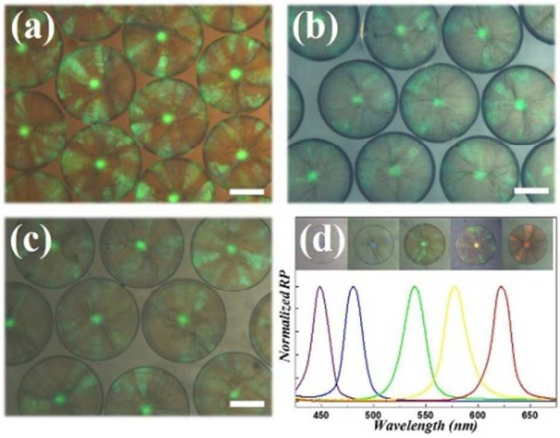

Fig. 2 Reflection images of (a) the SCCBs, (b) the MIP hydrogel hybrid SCCBs, and (c) the MIP inverse opal particles. Scale bars are 100 μm in (a-c). (d) Reflection peaks and reflection images of 5 different MIP inverse opal particles.

swelling of the hydrogel volume, the selectivity of the MIP materials to their targets was with undetectable influence. In our experiments, the diffraction peak shift (to red) of the MIP inverse opal particles is less than 15 nm, thus the particles can be encoded by the spectral ranges between their initial position of the diffraction peak to the red orientation of wavelengths 20 nm. Thus, more than 30 kinds of molecules, in theory, are generally enough for the demand of clinical diagnoses, can be detected simultaneously in the spectral range from 380 nm to 1000 nm by using the MIP inverse opal particles without code interference between each other.

As a proof of concept for the antibody- and label-free detection, horseradish peroxidase (HRP), ribonuclease B (RNase B), and transferrin (TRF) were used as the imprinted molecules in the boronate affinity MIP inverse opal particles, respectively. When an imprinted biomolecule enters a complementary nanocavity of the MIP inverse opal particles, a multitude of simultaneous hydrogen bonds can be formed between the oriented boronic groups in the nanocavity and the polar surface residues of the glycoprotein. These cooperative, multivalent hydrogen bonds lead to a significantly increased selective glycoprotein-binding affinity. During this process of molecular recognition, the specific binding of glycoprotein to the imprinted nanocavities of the MIP inverse opal particles not only lead to the swelling of the MIPs, but also increase the average refractive index of the particles (as the refractive index of the protein 1.42 is larger than that of water 1.33), and both are reported by the particles through a red-shift of the Bragg diffraction peak (Fig. 3).

Generally, it is beneficial for sensitive glycoprotein detection by using a MIP hydrogel with a high swelling ratio, which could be realized by adding porogen, reducing the concentration of pregel solution, or decreasing the ratio of cross-linkers. In our experiment, polyethylene glycol (PEG) molecule was employed as the porogen solution, which can occupy space in the MIP hydrogel without reacting with other ingredients. This improvement not only imparts the MIP hydrogel a porous structure, but also provides additional channels for the imprinted target molecules accessing. Although a high percentage of the PEG porogen would lead to a highly elastic

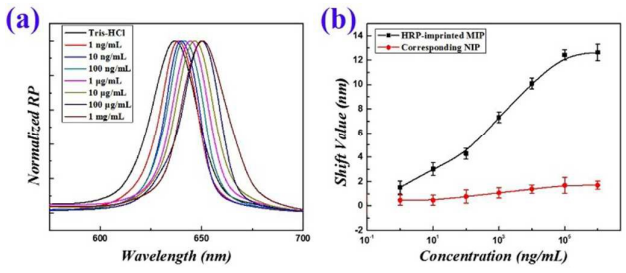

Fig. 3 (a) Optical response of the HRP imprinted inverse opal particles incubated in different concentrations of the target HRP. (b) Bragg diffraction peak shift values of the imprinted and non-imprinted inverse opal particles in different concentrations of the HRP. The number of replicates at any concentration was five.

MIP hydrogel, the mechanical strength of the hydrogel was decreased and the inverse opal structure of the particles became difficult to maintain (Fig. S2). Thus, a compromising PEG porogen concentration of 20% was employed. Under this condition, the concentration of the pregel solution and the ratio of the monomers to cross-linkers were optimized. It was found that the MIP hydrogel particles could reach an obvious red-shift of the Bragg diffraction peak under their corresponding imprinted glycoprotein when the MIP hydrogel were prepared with a concentration of PEGDA about 25% and a molar ratio of about 12:1 for the cross-linkers and the monomer. Remarkably, a trace amount of the analyte is sufficient to lead to a red-shift of the diffraction peak (Fig. 3a). Therefore, these concentrations and ratios were used to fabricate all the MIP hydrogel particles for the antibody- and label-free detection in the following experiment.

To investigate the specificity of this method, the MIP and non-molecularly imprinted polymer (NIP) inverse opal hydrogel particles with the same diffraction peak were incubated in the template solutions, respectively. It was found that only the MIP inverse opal hydrogel particles could report a red-shift of their Bragg diffraction peak, and the NIP particles had undetectable peak shifts (Fig. 3b and Fig. S3). This indicated the artificial probe feature of the MIP materials to their template molecules. The imprinting factor (6.9) and binding capacity (24.62nmol/g) also confirmed this feature of the MIP materials (Fig. S4). To further investigate the specificity of the MIP inverse opal hydrogel particles in protein recognition, HRP imprinted particles were tested with solutions of HRP, RNase B and TRF, respectively. Fig. 4a displays the optical response of the particles after being incubated in these solutions. It can be observed that the MIP inverse opal hydrogel particles specifically recognized their template biomolecule HRP and reported the recognition process as a red-shift of their Bragg diffraction peak, while displaying negligible response of their peak position to the control proteins. The RNase B and TRF imprinted inverse opal hydrogel particles also showed high specificity to their corresponding target template molecules (Fig. S5).

To demonstrate the multiplexing capabilities of the suspension array for the label-free detection of biomolecules, three kinds of encoded inverse opal hydrogel particles (encoded by red, orange, and green structural colors) with HRP, RNase B, and TRF imprinting, respectively, were prepared. These encoded MIP inverse opal hydrogel particles were then mixed together and incubated in an analyte solution containing HRP and RNase B. Fig. 4b shows the change of the diffraction peaks of the suspension array after the multiplex assay. It can be observed that only the red and orange structural colors encoded MIP hydrogel particles showed a red shift of their diffraction peak while the green particles displayed undetectable peak change. These results are consistent with the content of the sample to which the MIP inverse opal hydrogel particles were exposed. In this process, analyzing the spectral ranges of the measured diffraction peaks can lead to decoding, and the quantities of analytes can be estimated by the shift values of the peaks positions. Thus,

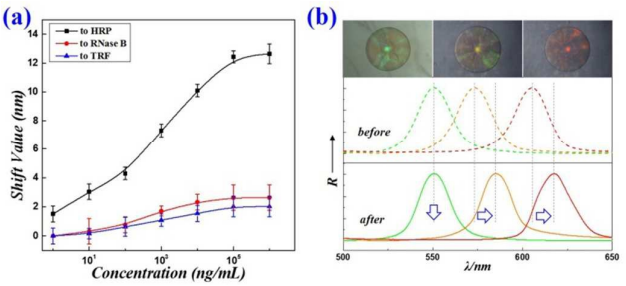

Fig. 4 (a) Plot of the Bragg shifts for the HRP imprinted inverse opal particles in response to solutions of HRP, RNase B, and TRF at different concentrations. The number of replicates at any concentration was five. Error bars represent standard deviations. (b) Reflection images (top) and reflection spectra (middle and bottom) of three kinds of MIP inverse opal particles before and after the multiplex assay. The green, orange, and red inverse opal particles were imprinted with TRF, RNase B and HRP, respectively. The middle dashed peaks and the bottom solid peaks are the reflection spectra of the MIP inverse opal particles before and after the detection.

only a simple one-step measurement of the diffraction peak of the MIP hydrogel particles is needed for both the decoding and biomolecule detection, which requires only some simple instruments and simplifies the procedure. As for real application, the TRF-imprinted MIP were prepared and used for detecting. It was found that the TRF in artificial urine, which has the same component as real urine, could still be detected with an excellent tolerance (Fig. S6). These results indicate the multiplexing capabilities of the encoded MIP hydrogel particles for practical applications.

In conclusion, we have incorporated a boronate affinity molecular imprinting technique to a suspension array and have demonstrated the concept of antibody- and label-free multiplex detection by using the suspension array. The barcode particles of our suspension array are inverse opal particles with boronate affinity MIP scaffolds. When used for detection, specific binding of the glycoprotein biomolecules in the imprinted boronate affinity nanocavities caused a readable red shift in the diffraction peak of the barcode particles, which can be used for directly detecting and decoding multiple biomolecules simultaneously. The detection results indicated the specificity and sensitivity of the MIP particle-based suspension array. These unique features of the boronate affinity MIP inverse opal barcode particles indicate that this new type of suspension array is very promising in overcoming many restrictions of current techniques, and thus it is anticipated to open new horizons in medical diagnostics.

This work was supported by the National Science Foundation of China (Grant Nos. 21473029, 81202250 and 51522302), the NASF Foundation of China (Grant No. U1530260), the National Science Foundation of Jiangsu (Grant No. BK20140028), and the Research Fund for the Doctoral Program of Higher Education of China (20120092130006).

Notes and references

1. (a) D. R. Walt, *Science*, 2000, **287**, 451-452. (b) J. Lee, P. W. Bisso, R. L. Srinivas, J. J. Kim, A. J. Swiston and P. S. Doyle, *Nat. Mater.*, 2014, **13**, 524-529. (c) L. Wang, M. B. O'Donoghue and W. H. Tan, *Nanomedicine-Uk*, 2006, **1**, 413-426. (d) N. G. Clack, K. Salaita and J. T. Groves, *Nat. Biotechnol.*, 2008, **26**, 825-830. (e) F. Y. Zheng, Y. Cheng, J. Wang, J. Lu, B. Zhang, Y. J. Zhao and Z. Z. Gu, *Adv. Mater.*, 2014, **26**, 7333-7338. (f) B. F. Ye, H. B. Ding, Y. Cheng, H. C. Gu, Y. J. Zhao, Z. Y. Xie and Z. Z. Gu, *Adv. Mater.*, 2014, **26**, 3270-3274. (g) Y. J. Zhao, Y. Cheng, L. R. Shang, J. Wang, Z. Y. Xie and Z. Z. Gu, *Small*, 2015, **11**, 151-174.
2. (a) R. Wilson, A. R. Cossins and D. G. Spiller, *Angew. Chem. Int. Edit.*, 2006, **45**, 6104-6117. (b) S. Birtwell and H. Morgan, *Integr. Biol.*, 2009, **1**, 345-362. (c) Y. Song, Y. K. Chan, Q. M. Ma, Z. Liu and H. C. Shum, *Acs Appl. Mater. Inter.*, 2015, **7**, 13925-13933.
3. (a) N. Christodoulides, S. Mohanty, C. S. Miller, M. C. Langub, P. N. Floriano, P. Dharshan, M. F. Ali, B. Bernard, D. Romanovicz, E. Anslyn, P. C. Fox and J. T. McDevitt, *Lab Chip*, 2005, **5**, 261-269. (b) N. Christodoulides, M. Tran, P. N. Floriano, M. Rodriguez, A. Goodey, M. Ali, D. Neikirk and J. T. McDevitt, *Anal. Chem.*, 2002, **74**, 3030-3036.
4. (a) M. Y. Han, X. H. Gao, J. Z. Su and S. Nie, *Nat. Biotechnol.*, 2001, **19**, 631-635. (b) D. Y. Wang, A. L. Rogach and F. Caruso, *Nano Lett*, 2002, **2**, 857-861.
5. (a) W. Liu, L. R. Shang, F. Y. Zheng, J. Lu, J. L. Qian, Y. J. Zhao and Z. Z. Gu, *Small*, 2014, **10**, 88-93. (b) Y. J. Zhao, L. R. Shang, Y. Cheng and Z. Z. Gu, *Accounts. Chem. Res.*, 2014, **47**, 3632-3642. (c) L. R. Shang, F. Q. Shangguan, Y. Cheng, J. Lu, Z. Y. Xie, Y. J. Zhao and Z. Z. Gu, *Nanoscale*, 2013, **5**, 9553-9557. (d) H. Hwang, S. H. Kim and S. M. Yang, *Lab Chip*, 2011, **11**, 87-92. (e) S. H. Kim, J. G. Park, T. M. Choi, V. N. Manoharan and D. A. Weitz, *Nat. Commun.*, 2014, **5**.
6. (a) M. Kuang, D. Y. Wang, H. B. Bao, M. Y. Gao, H. Mohwald and M. Jiang, *Adv. Mater.*, 2005, **17**, 267-270. (b) X. H. Gao and S. M. Nie, *Anal. Chem.*, 2004, **76**, 2406-2410.
7. (a) J. Hou, H. Zhang, Q. Yang, M. Li, L. Jiang and Y. Song, *Small*, 2015, **11**, 2738-2742. (b) Y. Zhang, J. Qiu, M. Gao, P. Li, L. Gao, L. Heng, B. Z. Tang and L. Jiang, *J. Mater. Chem. C.*, 2014, **2**, 8865-8872. (c) X. Hu, G. Li, J. Huang, D. Zhang and Y. Qiu, *Adv. Mater.*, 2007, **19**, 4327-4332. (d) J. P. Ge and Y. D. Yin, *Angew. Chem. Int. Edit.*, 2011, **50**, 1492-1522. (e) W. Chen, Y. Ma, J. M. Pan, Z. H. Meng, G. Q. Pan and B. Sellergren, *Polymers*, 2015, **7**, 1689-1715. (f) G. Q. Pan, Q. P. Guo, Y. Ma, H. L. Yang and B. Li, *Angew. Chem. Int. Edit.*, 2013, **52**, 6907-6911. (g) G. Q. Pan, Q. P. Guo, C. B. Cao, H. L. Yang and B. Li, *Soft Matter*, 2013, **9**, 3840-3850.
8. (a) L. Li, Y. Lu, Z. J. Bie, H. Y. Chen and Z. Liu, *Angew. Chem. Int. Edit.*, 2013, **52**, 7451-7454. (b) J. Ye, Y. Chen and Z. Liu, *Angew. Chem. Int. Edit.*, 2014, **53**, 10386-10389.
9. (a) X.D. Bi and Z.Liu, *Anal. Chem.*, 2014, **86**, 959–966. (b) X.D. Bi and Z.Liu, *Anal. Chem.*, 2014, **86**, 12382-12389.
10. (a) Z. J. Bie, Y. Chen, J. Ye, S. S. Wang, and Z. Liu, *Angew. Chem. Int. Edit.*, 2015, **54**, 10211-10215. (b) S.S. Wang, J. Ye, Z.J. Bie and Z. Liu. *Chem. Sci.*, 2014, **5**, 1135-1140.
11. X. B. Hu, G. T. Li, M. H. Li, J. Huang, Y. Li, Y. B. Gao and Y. H. Zhang, *Adv. Funct. Mater.*, 2008, **18**, 575-583.